Letter

Giant microwave sensitivity of a magnetic array by long-range chiral interaction driven skin effect

Tao Yu [1,*] and Bowen Zeng [2]

[1]*School of Physics, Huazhong University of Science and Technology, Wuhan 430074, China*

[2]*Department of Applied Physics, School of Physics and Electronics, Hunan University, Changsha 410082, China*

(Received 16 January 2022; revised 21 March 2022; accepted 26 April 2022; published 2 May 2022)

A non-Hermitian skin effect was observed in one-dimensional systems with short-range chiral interactions. A long-range chiral interaction mediated by traveling waves also favors the accumulation of energy, but has not yet exhibited non-Hermitian topology. Here, we find that the strong interference brought by the wave propagation is detrimental for accumulation. By the suppression of interference via the damping of traveling waves, we predict the non-Hermitian skin effect of magnetic excitation in a periodic array of magnetic nanowires that are coupled chirally via spin waves of a thin magnetic substrate. The local excitation of a wire at one edge by weak microwaves of magnitude $\sim\mu$T leads to a considerable spin-wave amplitude at the other edge, i.e., a remarkable functionality useful for the sensitive, nonlocal, and nonreciprocal detection of microwaves.

DOI: 10.1103/PhysRevB.105.L180401

Introduction. A chiral interaction, also known as nonreciprocal coupling, refers to the asymmetric coupling amplitude between the left and right objects [1], such as the asymmetric hopping amplitude between two nearest sites in the Hatano-Nelson model [2]. It has been successfully implemented to realize the non-Hermitian skin effect in one-dimensional systems, featured by a macroscopic number of eigenstates piling up at one end [3–9]. These states turn out to be topologically exceptional, showing an anomalous bulk-boundary correspondence that may be characterized by a generalized Brillouin zone [4,6], and are promising for applications such as the topological funneling of light [8].

Chirality is a common ingredient in topological magnetic orders [10–12], but in terms of which the realization of non-Hermitian topology is rarely addressed [13,14]. A chiral interaction between the Kittel magnons of a magnetic wire (or sphere) has been recently discovered when they couple with the traveling modes such as the spin waves in films [15–18], waveguide microwaves [19,20], and surface acoustic waves [21–23], to name a few, in that the Kittel modes prefer to couple with the traveling waves propagating in one direction. We have argued that these traveling waves can mediate a long-range chiral interaction between two magnetic wires if their damping is not large [17,18]. It could be thereby speculated that these long-range chiral interactions might lead to a non-Hermitian skin effect similar to that by the chiral short-range interaction in the Hatano-Nelson model [2] since the energy tends to accumulate at one end. However, a theoretical study showed that these systems do not favor the coalescence of bulk modes [19] but only hold a weak skin tendency for those modes with large decay rates, nor were the edge modes ever observed by experiments [18,24–26]. The interference brought by the propagation of the traveling waves is detrimental for the accumulation.

In this Letter, we propose the realization of a non-Hermitian topological phase in one-dimensional long-range coupled magnets by figuring out the collective role of the chirality and suppression of propagation interference via the damping of the interaction mediator. To be specific, we model an array of magnetic wires saturated along the wire direction on top of a thin magnetic film that are coupled via the dipolar interaction, as depicted in Fig. 1. When the film magnetization is along the wire direction, the coupling between the Kittel mode and the film spin waves is chiral in that the former only couples to the latter propagating in one direction [16], the chirality being tunable by the direction of the magnetization of the film [27]. The spin waves in the film then mediate a chiral interaction with an asymmetric coupling strength between the left and right wires. We find that when the damping of the spin waves of the film is *sufficiently strong* (while assuming the wire has a small damping), all the collective modes of the array of wires are localized at one edge, showing a non-Hermitian skin effect. This skin effect, however, vanishes when the damping tends to zero or the chirality is absent. We analytically approach the generalized Brillouin zone that characterizes a nontrivial winding of the eigenfrequency only when there exist both chirality and strong damping of the film spin waves. The non-Hermitian skin effect can act as a nonlocal and nonreciprocal information processor since the excitation of the wire at one edge leads to a large amplitude at the other edge. It is extremely sensitive, which allows for the detection of microwaves as small as μT, a functionality that may be implemented in classical information processing and future quantum technology.

Chiral interaction between objects. We consider a one-dimensional model with a periodic array of N magnetic nanowires of thickness d on a thin magnetic film of thickness s (Fig. 1) [18,24–26]. The distance between the neighboring wires L_0 is much larger than the wire width w such that the direct dipolar interaction between wires is negligible. The lth wire is centered at $\mathbf{r}_l = R_l\hat{\mathbf{y}} = lL_0\hat{\mathbf{y}}$. The saturated

*taoyuphy@hust.edu.cn

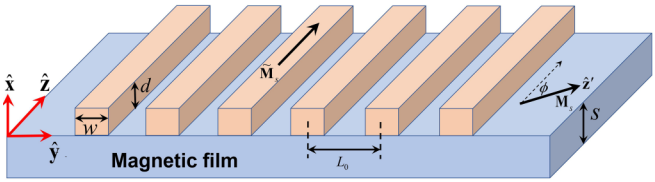

FIG. 1. A periodic array of magnetic nanowires on top of a thin magnetic film. The direction of the saturated magnetization of the wire is pinned along the $\hat{\mathbf{z}}$ direction, while the saturated magnetization of the film is tunable by the applied magnetic field in the film plane. The geometric parameters are given in the text.

magnetization $\tilde{\mathbf{M}}_s$ of the wire is pinned along the wire $\hat{\mathbf{z}}$ direction by shape anisotropy, while the film saturated magnetization $\mathbf{M}_s$ along $\hat{\mathbf{z}}'$ is tunable by the applied magnetic field $\mathbf{H}_{\rm app}$ with an angle ϕ with respect to the wire direction.

The interlayer exchange interaction between the wire and film is suppressed by an insulating spacer [18,24]. The magnetization $\tilde{\mathbf{M}}_l$ in the lth magnetic wire couples with the stray field $\mathbf{h}$ from $\mathbf{M}$ in the film via the dipolar interaction $\hat{H}_{\rm int} = -\mu_0 \int_0^d dx d\rho \tilde{\mathbf{M}}_{\mathbf{l},\alpha}(\mathbf{x},\rho)\mathbf{h}_\alpha(\mathbf{x},\rho)$, in the summation convention over repeated Cartesian indices $\alpha = \{x,y,z\}$, with μ_0 being the vacuum permeability. Focusing on the linear regime, the magnetization in the magnetic wires and film is expanded by the magnon operator [28,29],

$$\hat{M}_x(\mathbf{r}) = \sqrt{2M_s\gamma\hbar}\sum_k \left[m_x^{(k)}(x)e^{iky}\hat{a}_k + \text{H.c.}\right],$$

$$\hat{M}_y(\mathbf{r}) = \cos\phi\sqrt{2M_s\gamma\hbar}\sum_k \left[im_x^{(k)}(x)e^{iky}\hat{a}_k + \text{H.c.}\right],$$

$$\hat{\tilde{M}}_{\alpha=\{x,y\},l}(\mathbf{r}) = \sqrt{2\tilde{M}_s\gamma\hbar}\left[\tilde{m}^{\rm K}_{l,\alpha}(\mathbf{r})\hat{b}_l + \text{H.c.}\right], \quad (1)$$

where γ is the modulus of the gyromagnetic ratio, $m_x^{(k)}(x)$ and $\tilde{m}^{\rm K}_{l,\alpha}(\mathbf{r})$ represent the amplitude of the spin waves and Kittel modes, and $\hat{a}_k$ and $\hat{b}_l$ denote the magnon operators in the film and wire. For simplicity, k denotes k_y. The total Hamiltonian $\hat{H}/\hbar = \sum_l \omega_{\rm K}\hat{b}_l^\dagger\hat{b}_l + \sum_k \omega_k\hat{a}_k^\dagger\hat{a}_k + \sum_l\sum_k(g_k e^{-ikR_l}\hat{b}_l\hat{a}_k^\dagger + g_k e^{ikR_l}\hat{b}_l^\dagger\hat{a}_k)$ is expressed by the coupled harmonic oscillators [27,30]. Here, $\omega_{\rm K}$ is the frequency of the Kittel mode of the wires, and $\omega_k = \mu_0\gamma H_{\rm app} + \alpha_{\rm ex}\mu_0\gamma M_s k^2$ is the dispersion of the spin waves of the film with the slope governed by the exchange stiffness $\alpha_{\rm ex}$. The coupling constant $g_k = \mathcal{D}(k)m_x^{(k)*}(|k| + k\cos\phi)[\tilde{m}_x^{\rm K} + i\,\mathrm{sgn}(k)\tilde{m}_y^{\rm K}]$ depends on the propagation direction of the spin waves, the relative direction of the magnetization in the film and nanowire, and the geometry of the wire and film via the form factor $\mathcal{D}(k) = -2\mu_0\gamma\sqrt{M_s\tilde{M}_s/\Lambda}(1-e^{-|k|d})(1-e^{-|k|s})\sin(kw/2)/k^3$. Here, Λ is the length of the magnetic wire. The spin waves in the film are circularly polarized when their wavelength is sufficiently short [18,24,27]. Thereby when $\phi = 0$ ($\phi = \pi$), i.e., the magnetization of the wire and film is parallel (antiparallel), the wire Kittel mode only couples with the right-going (left-going) spin waves with $g_{-|k|} = 0$ ($g_{|k|} = 0$) [27].

These directional spin waves mediate a chiral interaction between two wires, approached by the Langevin equation. When the magnetic quality of the wire is higher than that of the film, we are allowed to use the Markov approximation [31,32]. Integrating out the film degree of freedom yields the Langevin equation for wires,

$$\frac{d\hat{b}_l}{dt} = -i\omega_{\rm K}\hat{b}_l - \frac{\kappa}{2}\hat{b}_l - G_l(\omega)\hat{b}_l - \sum_{l\neq l'} G_{ll'}(\omega)\hat{b}_{l'}. \quad (2)$$

It describes an effective interaction between the Kittel magnons at any instant by several coupling parameters. Here, $\kappa = 2\tilde{\alpha}_{\rm G}\omega_{\rm K}$ and $\kappa_k = 2\alpha_{\rm G}\omega_k$ are the Gilbert damping of the wire Kittel modes and film spin waves, respectively, parametrized by the Gilbert coefficient $\tilde{\alpha}_{\rm G}$ and $\alpha_{\rm G}$. Additional damping is induced by pumping the spin waves that lose energy with rates $G_l(\omega) \to (|g_{k_\omega}|^2 + |g_{-k_\omega}|^2)/[2v(k_\omega)]$, where $v(k) = 2\alpha_{\rm ex}\mu_0\gamma M_s k$ is the group velocity of the traveling waves and $k_\omega = \sqrt{(\omega-\mu_0\gamma H_{\rm app})/(\alpha_{\rm ex}\mu_0\gamma M_s)}$ is the positive root of $\omega_k = \omega$. The spin waves mediate an effective interaction $G_{ll'}(\omega)$ of finite range when taking into account the finite damping of spin waves. With the root $q_\omega = k_\omega(1 + i\alpha_G/2)$ of $\omega - \omega_k + i\kappa_k/2 = 0$,

$$G_{ll'}(\omega) = \frac{\Lambda}{v(k_\omega)}e^{iq_\omega|l-l'|L_0}\begin{cases}|g_{k_\omega}|^2, & R_l > R_{l'},\\ |g_{-k_\omega}|^2, & R_l < R_{l'}.\end{cases}$$

The interaction is of long range when $\alpha_G k_\omega L_0/2 \ll 1$. The constant $\Gamma_R = |g_{k_\omega}|^2/v(k_\omega)$ [$\Gamma_L = |g_{-k_\omega}|^2/v(k_\omega)$] represents the coupling strength from the left to right (right to left) wires.

Our predicted effect is not limited strongly by the material choice. Conventional materials such as cobalt wire may be suitable [18,24–26], but it has a relatively large damping. CoFeB has a relatively high magnetic quality [33,34] and large exchange stiffness [35–37]. We thus illustrate the effective couplings by exemplifying CoFeB wires of width $w = 150$ nm and thickness $d = 20$ nm on top of a Ni film of thickness $s = 5$ nm. With $\mu_0\tilde{M}_s = 0.6$ T for Ni [37] and $\mu_0 M_s = 1.6$ T [38] for CoFeB of stiffness $\alpha_{\rm ex} = 8\times 10^{-13}$ cm^2 [35,36], we plot the direction dependence of the coupling constants $\Gamma_{L,R}$ on the applied magnetic field of strength $\mu_0 H_{\rm app} = 0.1$ T in Fig. 2. With these parameters, the frequency of the Kittel modes of CoFeB wire is $\omega_{\rm K} = 60$ GHz [27]. The coupling is perfectly chiral when the magnetizations of the wire and film are parallel ($\Gamma_R \neq 0$ but $\Gamma_L = 0$) or antiparallel ($\Gamma_L \neq 0$ but $\Gamma_R = 0$). The chirality vanishes at two critical angles $\phi_c = \{0.4\pi, 1.6\pi\}$. Thereby, the system allows us to simulate rich physics from coupling with perfect chirality to coupling in the absence of chirality.

Non-Hermitian skin effect. Conveniently, the effective non-Hermitian Hamiltonian

$$\hat{H}_{\rm eff} = \left(\omega_{\rm K} - i\tilde{\alpha}_G\omega_{\rm K} - i\frac{\Gamma_R+\Gamma_L}{2}\right)\sum_{l=1}^{N}\hat{b}_l^\dagger\hat{b}_l - i\Gamma_R\sum_{l<l'}e^{iq_*|l-l'|L_0}\hat{b}_l^\dagger\hat{b}_{l'} - i\Gamma_L\sum_{l>l'}e^{iq_*|l-l'|L_0}\hat{b}_l^\dagger\hat{b}_{l'}, \quad (3)$$

recovers the Langevin equation (2), in which within the on-shell approximation $\Gamma_{L,R} \equiv \Gamma_{L,R}(\omega_{\rm K})$ and $q_* \equiv q_{\omega_{\rm K}}$. When $\tilde{\alpha}_G$ is small for the wire [33,34], the radiative damping $(\Gamma_R + \Gamma_L)/2$ by pumping the spin waves in the film dominates the damping of Kittel magnons. The Hamiltonian can be expressed via a non-Hermitian matrix $\tilde{H}_{\rm eff}$ via $\hat{H}_{\rm eff} = \hat{\Psi}^\dagger\tilde{H}_{\rm eff}\Psi$,

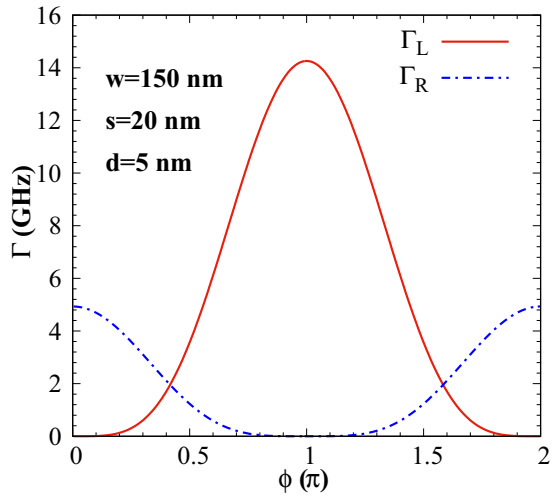

FIG. 2. Dependence of the coupling constants $\Gamma_{L,R}$ on the direction ϕ of the applied magnetic field. The geometric parameters are addressed in the figure, and the material parameters are given in the text.

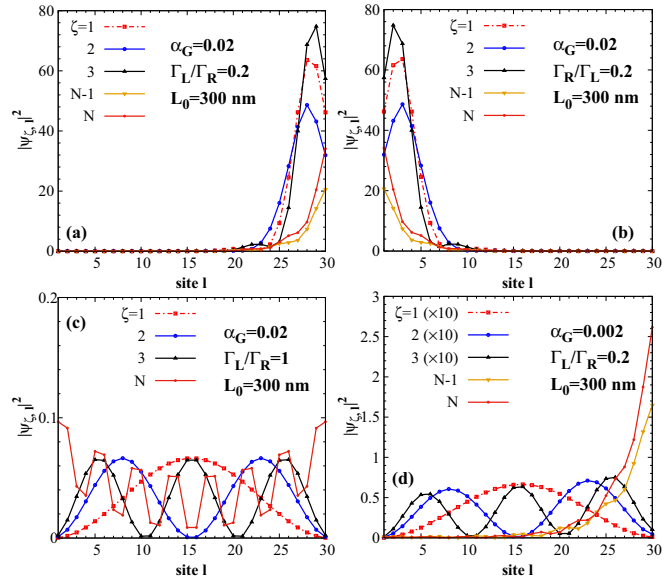

FIG. 3. Distribution of normalized eigenmodes under different conditions. All the modes are localized at the edge in (a) and (b) when the coupling is chiral and film damping is strong. The skin modes vanish either without chirality [(c)] or with weak film damping [(d)].

where $\hat{\Psi} = (\hat{b}_1, \hat{b}_2, \ldots, \hat{b}_N)^T$, with matrix elements

$$\tilde{H}_{\text{eff}}|_{ll'} = \begin{cases} \omega_{\text{K}} - i\tilde{\alpha}_G\omega_{\text{K}} - i(\Gamma_L + \Gamma_R)/2, & l = l', \\ -i\Gamma_L e^{iq_*(l-l')L_0}, & l > l', \\ -i\Gamma_R e^{iq_*(l'-l)L_0}, & l < l'. \end{cases} \quad (4)$$

The phase factor in the coupling constant comes from the propagation phase of the film spin waves, thus recording the interference of waves in the range limited by $1/|q_*|$. Although being a generalization of the Hatano-Nelson model, its topological property is, however, much less known than its short-range version. The right eigenvectors of $\tilde{H}_{\text{eff}}$ and $\tilde{H}^\dagger_{\text{eff}}$ are $\{\psi_\zeta\}$ and $\{\phi_\zeta\}$ with corresponding eigenvalues $\{\nu_\zeta\}$ and $\{\nu^*_\zeta\}$, where ζ is labeled from 1 to N by increasing their decay rates. $\phi^\dagger_\zeta$ is then a left eigenvector of $\tilde{H}_{\text{eff}}$. After normalization we have biorthonormality $\psi^\dagger_\zeta\phi_{\zeta'} = \delta_{\zeta\zeta'}$.

With the material parameters in Fig. 2, the resonant spin waves have a wave vector $k = 2\pi/88.9\ \text{nm}^{-1}$. When taking the Gilbert damping $\alpha_G = 0.02$ for Ni, the range of the spin-wave mediated interaction is $1/\text{Im}(q_*) = 1.41\ \mu$m. The interaction is of long range by choosing the distance of neighboring wires $L_0 = 300$ nm. The chirality is freely tunable by changing the direction of magnetization in the film plane as in Fig. 2. Here, we typically choose $\phi = \{0.3\pi, 0.54\pi\}$ that renders $\Gamma_L/\Gamma_R = 0.2$ and $\Gamma_R/\Gamma_L = 0.2$ for addressing the physics. In Fig. 3(a), all the modes are localized at the right edge when $\Gamma_R > \Gamma_L$, but become localized at the left edge when the chirality is reversed with $\Gamma_L > \Gamma_R$ as in Fig. 3(b). The skin effect vanishes without the chirality at the critical angle $\phi_c = 0.416\pi$, as shown in Fig. 3(c) where there are only few modes that have considerable amplitudes at the two edges, which have faster decay rates than the other modes as revealed via our further calculation. Also, localization vanishes when taking $\alpha_G = 2 \times 10^{-3}$ [Fig. 3(d)] [19]. Profoundly, the mode amplitudes are enhanced by two orders in magnitude by the skin effect. This is because these skin modes are in proximity to the Nth order exceptional points with a coalescence of all eigenvectors [3,39] when one of $\Gamma_{L,R}$ is exactly zero.

It is not trivial to find an analytical solution for the wave function that allows us to explicitly depict the generalized Brillouin zone, i.e., the distribution of complex momentum κ, parametrized by $\beta_k \equiv e^{ikL_0}$, on a complex plane [4,6]. We construct a Bloch state for a complex momentum as a traveling wave $\hat{\Psi}_\kappa = (1/\sqrt{N})\sum_{l=1}^N(\beta_\kappa)^l\hat{b}_l$, obeying, under Hamiltonian (3), the equation of motion $d\hat{\Psi}_\kappa/dt = -i\omega_\kappa\hat{\Psi}_\kappa - \Gamma_L g_\kappa\hat{\Psi}_{q_*} + \Gamma_R h_\kappa\hat{\Psi}_{-q_*}$ [19,40,41]. The dispersion relation

$$\omega_\kappa = (1 - i\tilde{\alpha}_G)\omega_{\text{K}} - i\frac{\Gamma_R}{2}\frac{1+\beta_\kappa\beta_{q_*}}{1-\beta_\kappa\beta_{q_*}} + i\frac{\Gamma_L}{2}\frac{1+\beta_\kappa\beta_{-q_*}}{1-\beta_\kappa\beta_{-q_*}}$$

is singular when $\kappa = \pm q_*$, implying that around these points the states have large decay rates. The traveling modes are not the eigenstates because of the existence of two edges in the chain that radiate energy with amplitudes $g_\kappa = 1/(1-\beta_\kappa\beta_{-q_*})$ and $h_\kappa = (\beta_\kappa)^N(\beta_{q_*})^N/(1-\beta_\kappa\beta_{q_*})$, and reflect the traveling modes. Thus we may superpose two traveling modes of the same energy with different momenta, i.e., $\omega_\kappa = \omega_{\kappa'}$ for a new mode. Superposition $\hat{\Delta} = g_{\kappa'}\hat{\Psi}_\kappa - g_\kappa\hat{\Psi}_{\kappa'}$ obeys

$$d\hat{\Delta}/dt = -i\omega_\kappa\hat{\Delta} + \Gamma_R(g_{\kappa'}h_\kappa - g_\kappa h_{\kappa'})\hat{\Psi}_{-q_*}, \quad (5)$$

and becomes the eigenmode when $g_{\kappa'}h_\kappa = g_\kappa h_{\kappa'}$. These are the desired relations to find the complex momentum κ and dispersion. Numerically diagonalizing the Hamiltonian with eigenfrequency ω_κ solves the complex momentum $\beta^{(\pm)}_\kappa = (-C_\kappa \pm \sqrt{C^2_\kappa - 4A_\kappa B_\kappa})/(2A_\kappa)$, containing two roots of momentum κ and κ' at the same frequency, where with $\tilde{\omega}_\kappa \equiv$

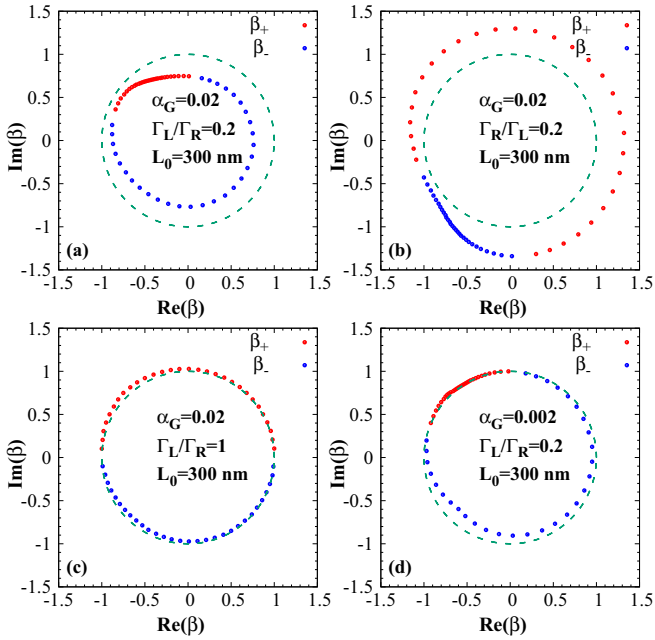

FIG. 4. Generalized Brillouin zone under different chiralities and dampings. $|\beta| < 1$ ($|\beta| > 1$) in (a) and (b) favors the localization at the right and left edges, respectively, while $|\beta| \approx 1$ in (c) and (d) indicates the absence of the skin effect.

$\omega_\kappa - \omega_{\rm K} + i\tilde{\alpha}_G\omega_{\rm K}$,

$$A_\kappa = \tilde{\omega}_\kappa - i(\Gamma_R - \Gamma_L)/2, \quad B_\kappa = \tilde{\omega}_\kappa + i(\Gamma_R - \Gamma_L)/2,$$

$$C_\kappa = -\left(\tilde{\omega}_\kappa - i\frac{\Gamma_R + \Gamma_L}{2}\right)\beta_{q_*} - \left(\tilde{\omega}_\kappa + i\frac{\Gamma_R + \Gamma_L}{2}\right)\beta_{-q_*}.$$

For the eigenmodes we expand $\hat{\Delta} = \sum_l \phi^*_{\zeta,l}\hat{b}_l$ and find the wave function

$$\psi_{\zeta,l} = C\left(g_{\kappa'}\beta_\kappa^{N-l} - g_\kappa\beta_{\kappa'}^{N-l}\right) \tag{6}$$

to be normalized with a constant C. The exponent $(N-l)$ controls the distribution of the excited wire magnons. When $|\beta_\kappa| > 1$ ($|\beta_\kappa| < 1$), the amplitude of $\psi_{\zeta,l}$ decreases (increases) with increasing the sites from 1 to N, implying the localization at the left (right) edge of the chain. Figure 4 plots the distribution of the real and imaginary parts of $\beta_\pm$, which form a loop in the complex plane, under different conditions. When there is net chirality and strong damping of the film, $|\beta_\pm|$ labeled by the red and blue dots deviate strongly from the unit that is indicated by the green dashed line. This is the condition for the emergence of the non-Hermitian skin effect [4,6]. When the chirality vanishes or the damping of the film becomes small, the distribution of β almost overlaps with the unit circle, indicating the absence of the skin effect.

Sensitive detection of microwaves. The wires can be excited and detected by the local metal stripline with a comparable width to w that is assumed to support a uniform electric current in the cross section [18]. A thin stripline on top of the (l_e)th wire generates a magnetic field $h_y\hat{\mathbf{y}}$ of frequency ω_d that locally excites beneath it the wire. The interaction between the field and wire Kittel mode $\hat{H}'_{\rm int} = \hbar(g_{l_e}e^{-i\omega_d t}\hat{\beta}^\dagger_{l_e} + {\rm H.c.})$ is parametrized by $g_{l_e} = -\mu_0\sqrt{\tilde{M}_s\gamma/(2\hbar)}h_y d w\tilde{m}^{\rm K}_{l_e,y}$. At the steady state, the excited amplitude of the magnetization in every wire follows $\langle\hat{\Psi}\rangle = \sum_\zeta g_{l_e}\phi^\dagger_{\zeta,l_e}\psi_\zeta/(\omega_d - \gamma_\zeta)$. To be realistic, we take into account the disorder modeled by the random shift $\delta\omega \in [-0.01\omega_{\rm K}, 0.01\omega_{\rm K}]$ to the Kittel frequency of every wire. The skin effect turns out to be robust to this disorder. To efficiently excite the localized modes at one edge, the local microwave source should locate at the other edge, i.e., nonlocal and nonreciprocal excitation. On the other hand, the mode amplitudes are greatly enhanced by the skin effect as in Fig. 3, leading to the expectation of sensitive microwave detection. Figure 5(a) is the numerical substantiation of the above expectation: A small microwave field 10 μT of frequency $\omega_d = 60$ GHz leads to a deviation of the magnetization $2\mu_0\sqrt{2\tilde{M}_s\gamma\hbar n_l}\tilde{m}_{l,y} = 0.09$ T of CoFeB wire with $\tilde{\alpha}_G = 0.01$ [33,34] at the steady state, i.e., a precession cone angle of $\sim 3.3^\circ$, n_l being the excited magnon number in the lth wire. The results converge when averaging up to 10^4 samples with random disorder.

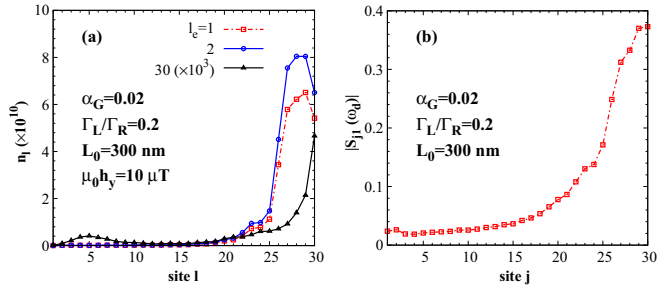

FIG. 5. Nonlocal excitation [(a)] and detection [(b)] of magnons by weak microwaves. In (a) the excited magnons accumulate at the right edge when the stripline locally excites the (l_e)th wire. (b) plots the microwave transmission when one antenna excites the wire at the left edge and the other antenna detects the signature above the jth wire.

For the experimental detection, the magnon density n_l in every wire can be directly measured by Brillouin light scattering [42,43] and nitrogen-vacancy (NV) center magnetometry [44,45]. Here, we predict the signature for the microwave transmission when placing one antenna above the wire at the left edge and the other above the jth wire. The transmission of a microwave of frequency ω_d is calculated via the input-output theory [31,32] that reads $S_{j1}(\omega_d) = -i\kappa_p\sum_\zeta \phi^\dagger_{\zeta,1}\psi_{\zeta,j}/(\omega_d - \gamma_\zeta)$, where κ_p is the radiative damping induced by the antenna. When taking $\kappa_p = 2\pi \times 10$ MHz [43], the distribution of $|S_{j1}(\omega_d)|$ in Fig. 5(b), after being averaged with the disorder, clearly shows the localization at the right edge.

Discussion. The array of magnetic wires over yttrium iron garnet was widely used as a magnetic antenna to excite the spin waves [24–26]. Recently, it became a platform for realizing the long-range chiral interaction between magnon of the wires as predicted theoretically [16,17] and measured experimentally [18,24], which, however, only supports very few slightly localized modes at the edge that renders the difficulty to accumulate all the excitations [19]. We achieve an advancement to realize the localization of *all the magnon modes at one edge*, which only needs to replace the yttrium iron garnet substrate by conventional magnetic materials of normal damping in the mature setups [24–26]. Such a

localization of all bulk modes comes from the non-Hermitian skin effect with a topological origin, which thereby allows for some unavoidable disorders.

Our method for setting up an effective Hamiltonian by integrating out the other degree of freedom is similar to that via the calculation of self-energy of interacting magnons [46] or electrons [47]. Different from the obtained non-Hermitian Weyl physics that has robust exceptional points [46,47], our results add an important vision that a magnetic hybridized system can support a nontrivial non-Hermitian effect accompanied by the skin effect without any exceptional point, which may bring functionalities such as nonlocal spin-wave excitation, sensitive detection of microwaves, and achieving a nonlinear regime of magnons with a small power. The generalization of our scenario to chiral photonics [1,48], plasmonics [49–51], and acoustics [52,53] may promote the performance of sensors for the detection of small signals.

Acknowledgments. This work is financially supported by the National Natural Science Foundation of China and the startup grant of Huazhong University of Science and Technology (Grants No. 3004012185 and No. 3004012198). B.Z. is financially supported by the National Natural Science Foundation of China Grant No. 12004106. We thank Gerrit E. W. Bauer, Yu-Xiang Zhang, and Jian-Song Pan for useful discussions.

[1] P. Lodahl, S. Mahmoodian, S. Stobbe, A. Rauschenbeutel, P. Schneeweiss, J. Volz, H. Pichler, and P. Zoller, Nature (London) **541**, 473 (2017).
[2] N. Hatano and D. R. Nelson, Phys. Rev. Lett. **77**, 570 (1996).
[3] E. J. Bergholtz, J. C. Budich, and F. K. Kunst, Rev. Mod. Phys. **93**, 015005 (2021).
[4] S. Yao and Z. Wang, Phys. Rev. Lett. **121**, 086803 (2018).
[5] Z. Gong, Y. Ashida, K. Kawabata, K. Takasan, S. Higashikawa, and M. Ueda, Phys. Rev. X **8**, 031079 (2018).
[6] Z. Yang, K. Zhang, C. Fang, and J. Hu, Phys. Rev. Lett. **125**, 226402 (2020).
[7] T. Helbig, T. Hofmann, S. Imhof, M. Abdelghany, T. Kiessling, L. W. Molenkamp, C. H. Lee, A. Szameit, M. Greiter, and R. Thomale, Nat. Phys. **16**, 747 (2020).
[8] S. Weidemann, M. Kremer, T. Helbig, T. Hofmann, A. Stegmaier, M. Greiter, R. Thomale, and A. Szameit, Science **368**, 311 (2020).
[9] K. Wang, A. Dutt, K. Y. Yang, C. C. Wojcik, J. Vuckovic, and S. Fan, Science **371**, 1240 (2021).
[10] W. J. Jiang, G. Chen, K. Liu, J. D. Zang, S. G. E. te Velthuis, and A. Hoffmann, Phys. Rep. **704**, 1 (2017).
[11] S.-H. Yang, Appl. Phys. Lett. **116**, 120502 (2020).
[12] S.-H. Yang, R. Naaman, Y. Paltiel, and S. S. P. Parkin, Nat. Rev. Phys. **3**, 328 (2021).
[13] B. Flebus, R. A. Duine, and H. M. Hurst, Phys. Rev. B **102**, 180408(R) (2020).
[14] K. Deng and B. Flebus, arXiv:2109.01711.
[15] Y. Au, E. Ahmad, O. Dmytriiev, M. Dvornik, T. Davison, and V. V. Kruglyak, Appl. Phys. Lett. **100**, 182404 (2012).
[16] T. Yu, C. P. Liu, H. M. Yu, Y. M. Blanter, and G. E. W. Bauer, Phys. Rev. B **99**, 134424 (2019).
[17] T. Yu, H. Wang, M. A. Sentef, H. M. Yu, and G. E. W. Bauer, Phys. Rev. B **102**, 054429 (2020).
[18] H. C. Wang, J. L. Chen, T. Yu, C. P. Liu, C. Y. Guo, H. Jia, S. Liu, K. Shen, T. Liu, J. Y. Zhang, M. A. Cabero, Q. M. Song, S. Tu, L. Flacke, M. Althammer, M. Weiler, M. Z. Wu, X. F. Han, K. Xia, D. P. Yu, G. E. W. Bauer *et al.*, Nano Res. **14**, 2133 (2021).
[19] T. Yu, X. Zhang, S. Sharma, Y. M. Blanter, and G. E. W. Bauer, Phys. Rev. B **101**, 094414 (2020).
[20] X. F. Zhang, A. Galda, X. Han, D. F. Jin, and V. M. Vinokur, Phys. Rev. Applied **13**, 044039 (2020).
[21] T. Yu, Phys. Rev. B **102**, 134417 (2020).
[22] M. R. Xu, K. Yamamoto, J. Puebla, K. Baumgaertl, B. Rana, K. Miura, H. Takahashi, D. Grundler, S. Maekawa, and Y. Otani, Sci. Adv. **6**, eabb1724 (2020).
[23] K. Yamamoto, W. C. Yu, T. Yu, J. Puebla, M. R. Xu, S. Maekawa, and G. E. W. Bauer, J. Phys. Soc. Jpn. **89**, 113702 (2020).
[24] H. C. Wang, M. Madami, J. L. Chen, L. T. Sheng, M. K. Zhao, Y. Zhang, W. Q. He, C. Y. Guo, H. Jia, S. Liu, Q. M. Song, X. F. Han, D. P. Yu, G. Gubbiotti, and H. M. Yu, ACS Nano **15**, 9076 (2021).
[25] C. P. Liu *et al.*, Nat. Commun. **9**, 738 (2018).
[26] P. Che, K. Baumgaertl, A. Kúkol'ová, C. Dubs, and D. Grundler, Nat. Commun. **11**, 1445 (2020).
[27] T. Yu, Y. M. Blanter, and G. E. W. Bauer, Phys. Rev. Lett. **123**, 247202 (2019).
[28] T. Holstein and H. Primakoff, Phys. Rev. **58**, 1098 (1940).
[29] A. Kamra and W. Belzig, Phys. Rev. Lett. **116**, 146601 (2016).
[30] J. D. Jackson, *Classical Electrodynamics* (Wiley, New York, 1998).
[31] C. W. Gardiner and M. J. Collett, Phys. Rev. A **31**, 3761 (1985).
[32] A. A. Clerk, M. H. Devoret, S. M. Girvin, F. Marquardt, and R. J. Schoelkopf, Rev. Mod. Phys. **82**, 1155 (2010).
[33] S. Iihama, S. Mizukami, H. Naganuma, M. Oogane, Y. Ando, and T. Miyazaki, Phys. Rev. B **89**, 174416 (2014).
[34] D. M. Lattery, D. Zhang, J. Zhu, X. Hang, J.-P. Wang, and X. Wang, Sci. Rep. **8**, 13395 (2018).
[35] H. A. Mook, J. W. Lynn, and R. M. Nicklow, Phys. Rev. Lett. **30**, 556 (1973).
[36] M. Pajda, J. Kudrnovský, I. Turek, V. Drchal, and P. Bruno, Phys. Rev. B **64**, 174402 (2001).
[37] J. L. Chen, C. P. Liu, T. Liu, Y. Xiao, K. Xia, G. E. W. Bauer, M. Z. Wu, and H. M. Yu, Phys. Rev. Lett. **120**, 217202 (2018).
[38] M. Küß, M. Heigl, L. Flacke, A. Hörner, M. Weiler, M. Albrecht, and A. Wixforth, Phys. Rev. Lett. **125**, 217203 (2020).
[39] W. D. Heiss, J. Phys. A: Math. Theor. **45**, 444016 (2012).
[40] Y.-X. Zhang and K. Mølmer, Phys. Rev. Lett. **122**, 203605 (2019).
[41] Y.-X. Zhang and K. Mølmer, Phys. Rev. Lett. **125**, 253601 (2020).
[42] S. O. Demokritov, B. Hillebrands, and A. N. Slavin, Phys. Rep. **348**, 441 (2001).

[43] J. L. Chen, T. Yu, C. P. Liu, T. Liu, M. Madami, K. Shen, J. Y. Zhang, S. Tu, M. S. Alam, K. Xia, M. Z. Wu, G. Gubbiotti, Y. M. Blanter, G. E. W. Bauer, and H. M. Yu, Phys. Rev. B **100**, 104427 (2019).

[44] T. van der Sar, F. Casola, R. L. Walsworth, and A. Yacoby, Nat. Commun. **6**, 7886 (2015).

[45] I. Bertelli, J. J. Carmiggelt, T. Yu, B. G. Simon, C. C. Pothoven, G. E. Bauer, Y. M. Blanter, J. Aarts, and T. van der Sar, Sci. Adv. **6**, eabd3556 (2020).

[46] P. A. McClarty and J. G. Rau, Phys. Rev. B **100**, 100405(R) (2019).

[47] E. J. Bergholtz and J. C. Budich, Phys. Rev. Research **1**, 012003(R) (2019).

[48] L. Novotny and B. Hecht, *Principles of Nano-Optics* (Cambridge University Press, Cambridge, UK, 2006).

[49] F. J. Rodríguez-Fortuño, G. Marino, P. Ginzburg, D. O'Connor, A. Martínez, G. A. Wurtz, and A. V. Zayats, Science **340**, 328 (2013).

[50] K. Y. Bliokh, D. Smirnova, and F. Nori, Science **348**, 1448 (2015).

[51] K. Y. Bliokh and F. Nori, Phys. Rep. **592**, 1 (2015).

[52] H. Nassar, B. Yousefzadeh, R. Fleury, M. Ruzzene, A. Alú, C. Daraio, A. N. Norris, G. Huang, and M. R. Haberman, Nat. Rev. Mater. **5**, 667 (2020).

[53] C. Rasmussen, L. Quan, and A. Alú, J. Appl. Phys. **129**, 210903 (2021).